CHARACTERIZATION OF COLD CATHODE EROSION PROCESSES

J.E. Polk*, A.J. Kelly†, R.G. Jahn‡
Electric Propulsion Laboratory
Princeton University, Princeton, NJ 08544

88-075

Abstract

Measurements of MPD thruster cathode erosion for six different current levels at one mass flow rate using a new mass loss detection system called Surface Layer Activation indicate that the cathode erosion rate follows an exponential dependence on the total arc current for currents below a critical point identified as the transition to full ionization. At this point the erosion rate increases by an order of magnitude from that at lower currents, then deviates from the exponential behavior in a drop to an intermediate level. The increase in erosion at the full ionization current is interpreted as a manifestation of an additional mass loss mechanism excited at that point. A related experiment designed to provide preliminary data on the characteristic length scale associated with cratering damage in cold cathode erosion by photomicrography of an arced cathode surface yielded a mean crater diameter of about 1 μm. The diameter of the observed craters was quite uniform over the cathode surface, indicating that the crater formation processes are relatively insensitive to changes in the discharge occurring along the cathode axis. A simple thermal model of crater formation yields a linear relationship between the diameter and the site current. This relationship coupled with measurements of crater densities suggests that individual emission sites on the cathode surface carry only a few amps and survive for about 100 nsec.

Introduction

The use of magnetoplasmadynamic (MPD) thrusters inherently involves long burn times on the order of 10^7 seconds to impart useful impulses to spacecraft, thus placing large demands on thruster component integrity. The cathode has been identified as the life-limiting component for operation below a critical current at which anode and insulator erosion prevent practical operation[1,3]. Nevertheless, cathode erosion research has been crippled by a lack of fundamental data and inability to identify the important parameters and processes. A research effort at the Princeton Electric Propulsion Laboratory has been concentrated on obtaining a database of fundamental cathode mass loss data and understanding the physical processes involved in cathode degradation.

Cathodes in MPD thrusters operate in two distinct modes which involve very different erosion processes. When the bulk cathode temperature is low, during quasi-steady operation and during the first few seconds of continuous operation, electrons are liberated mainly from a large number of very small, highly mobile emission sites. In these sites extremely high local temperatures, electric fields, and pressures cause local melting and ejection of cathode material. These local hot spots tend to damage the surface in the form of tiny hemispherical craters and molten tracks. This "spot" or "cold cathode" mode is found to be extremely destructive and limits cathode lifetime to around 10^5 seconds[1-9]. Despite this, efforts continue to develop quasi-steady thrusters with cold cathodes that can satisfy projected mission requirements.

During steady-state operation however, when the discharge heats the cathode to sufficiently high temperatures, a diffuse attachment with much lower current densities attributable to field-enhanced thermionic emission is observed. This "diffuse" or "hot cathode" mode has a much lower associated erosion rate that can be attributed primarily to evaporation[3]. A detailed grasp of the fundamental physical processes underlying both of these longevity limiting phenomena is an essential prerequisite for the development of engineering design criteria.

The first goal of the Princeton program is the development of the necessary tools to study cathode erosion processes. As a result of this effort the Surface Layer Activation (SLA) technique has been developed. Since this technique is described in detail elsewhere[1,2], it will be only briefly reviewed in this paper. The second goal involves simple modelling and collection of a broad database of erosion measurements correlated with other parameters for the spot and diffuse modes of cathode operation. A number of erosion measurements have been made on different thruster configurations and different operating conditions[1-9], but heretofore no attempt has been made to systematically study the effect of gross operating conditions such as total current, current density, mass flow rate, propellant species, cathode material and temperature on mass loss rates in MPD thrusters.

This paper contains a preliminary collection of erosion rates measured on the cold cathode of a quasi-steady MPD thruster for a range of total currents. Although the development of this experimental database is an essential first step, it is unlikely that erosion rate data alone will provide the insight necessary to understand the complex processes involved in cold cathode erosion. To evaluate the relative importance of the various heat inputs responsible for the destructive spot operation and to calculate the particle fluxes in the spot, the characteristic length scale over which spot parameters such as current density, surface temperature, and electric field can be considered constant must be determined. One approach to obtaining such data, photomicrography of arced cathodes, will be discussed. Comparison of crater length scales measured in an exploratory photomicrographic examination of a cathode surface arced by a single short discharge with the predictions of a simple model of crater formation show this to be a promising technique. Preliminary conclusions about cold cathode operation based on these first steps will then be presented.

Experimental Apparatus and Procedures

For this series of experiments the coaxial thruster configuration shown in Figure 1 was chosen. This design is based on the half-scale benchmark thruster[10] with a simplified mass injection system[11], improved insulation and active cooling of some components to allow quasi-steady operation with the cathode maintained at incandescent temperatures. In this thruster, a high speed solenoid valve controls the injection of argon through the boron nitride backplate via an annulus surrounding the central cathode and by 12 small holes arrayed on a circle near the quartz sidewall. The thruster was mounted in a fiberglass vacuum tank 1.8 m in diameter and 4.8 m long, which was typically maintained at a pressure of about 3×10^{-5} torr. Two msec duration rectangular current pulses were supplied through SCR switches by a 3000 μF, 175 kJ pulse-forming network.

Mass Loss Measurements

The amount of mass lost from the cathode surface is monitored with a new diagnostic technique called Surface Layer Activation (SLA)[1,2,12]. This method relies on the production of a radioactive tracer in a thin surface layer of the cathode by nuclear activation. The activity level of the tracer can then be monitored by observing the highly penetrating gamma radiation with standard radiation diagnostics mounted outside the thruster, and the decrease in activity during operation related to the amount of cathode material lost from the thin layer by erosion. This technique can provide highly accurate, in-situ, temporally and spatially resolved mass loss measurements in a few hundred shots or several minutes of continuous operation and can be applied to a wide range of materials.

The radioisotope used as a tracer is generated by bombarding a small spot on the cathode surface with a high energy ion beam in the Princeton University Cyclotron. In this experiment a spot approximately 5 mm long, 2 mm wide halfway along the length of the pure tungsten cathode was bombarded with a 15 MeV deuteron beam at an incident angle of 75°, which produced approximately 3.4 μCi of ^{184}Re in a layer about 33 μm deep with a dose of 3×10^{16} cm^{-2}. Typically 2% thoriated cathodes are used; however, with thoriated cathodes the surface coverage by thorium metal, and consequently the work function, cannot be easily determined. Pure tungsten with its more well defined work function was therefore used to avoid this ambiguity

---

*Graduate Student, AIAA Member
†Senior Research Engineer, AIAA Member
‡Professor, AIAA Fellow

in the mass loss measurements. Figure 2 is an autoradiograph of the cathode showing the position and extent of the activated area. The location was chosen to avoid the cathode base, where severe cracking and gross melting which could potentially distort the measurements by punching through the activated layer is often observed, and the hemispherical tip where surface curvature affects the interpretation of the data. The beam parameters were chosen on the basis of criteria which previous work[2] with this technique revealed are essential if accurate data are to be obtained.

The low level gamma radiation is not significantly attenuated by the thruster body, so the activity remaining in the surface layer can be measured with radiation detection equipment mounted near the thruster inside the vacuum tank. A Bicron 4x5 inch NaI(Tl) scintillator crystal with a photomultiplier tube base and preamplifier is mounted inside and electrically isolated from an aluminum cylinder containing atmospheric pressure to prevent arc attachment to the grounded electronics during thruster firing. Gamma rays absorbed by the crystal produce a number of photons proportional to the gamma energy. The photons are detected with the PM tube, which produces corresponding voltage pulses that are then read by an analog-to-digital converter and displayed as the number of detected decay events (counts) in a particular energy range (channel) by a Canberra Series 35 multichannel analyzer. Figure 3 shows several gamma spectra obtained by this method. The lower curve is the laboratory background. The highest curve is from the activated cathode and displays a number of low energy photopeaks belonging to ^{183}Re and ^{184}Re, the two long-lived isotopes produced by the deuteron bombardment, and the two higher energy photopeaks that are a composite of the three strongest lines in the ^{184}Re spectrum. The intermediate spectrum is from the same cathode after approximately 25% of the activated layer was removed by erosion.

Several methods can be used to determine the activity level of the cathode relative to the initial activity from the gamma spectra. The activity level is proportional to the rate of decay events, or the countrate, so a very simplistic method of analysis is to sum the counts in a particular spectral region and subtract the counts due to background radiation. The collection time can then be used to determine a countrate to be compared with the initial countrate. A more reliable estimate of the relative activity relies on the fact that the shape of the spectrum is constant, but the magnitude scales directly with the activity level, as can be seen qualitatively in the upper two spectra of Figure 3. The scaling parameter, or the relative activity, can be estimated by a least-squares analysis of a sample spectrum compared to a reference spectrum taken before any mass loss has occurred[13-15]. This method has been found to give the relative activity with an standard error of less than 0.5%. This activity change can be used to determine the total mass loss integrated over that period of operation.

Real time, time-resolved erosion measurements can be made by monitoring the total counts in a particular spectral range as a function of time, instead of analyzing the spectrum resulting after a series of discharges. The decrease in the counting rate with time is then a direct measure of the loss of material with time. The Canberra multichannel analyzer can be programmed to operate in this multichannel scaling (MCS) mode. Upper and lower level discriminators can be set to filter out all pulses above and below certain limits, so that particular spectral regions can be isolated, as shown in Figure 4 where the pulse height range has been set to contain just the two most intense photopeaks, thereby maximizing signal-to-noise ratio. The MCA then displays the total counts detected in a certain dwell time in successive channels to give an activity time history such as than shown in Figure 5, where each channel gives the counts detected in a 30 second dwell time. The plateaus in the data plotted in Figure 5 represent the unchanging countrate measured before and after the experiment, and the region with negative slope gives the decrease in countrate during a sequence of 250, two msec long discharges at 3 g/s and 12.35 kA at a repetition rate of 1 shot every 30 seconds. The absolute countrate is calculated by dividing the counts in each channel by the dwell time, and the relative countrate is determined by subtracting a background countrate for that spectral range and dividing by the initial countrate. The dwell time per channel can be varied from microseconds to hours to give a sufficiently high number of counts per channel and sufficient time resolution for the erosion process being studied. The uncertainty in the measured rate can be made arbitrarily low by increasing the activity level or the dwell time, but standard errors of a few percent have been attained with activity levels of a few μCi, dwell times of several 10's of seconds, and several hundred discharges.

The relationship between the observed change in activity and the amount of mass lost from the surface depends on the distribution of the radioactive tracer in the tungsten. In practice, this relationship is determined empirically in the form of a depth calibration curve such as that shown in Figure 6, which shows the depth or mass loss per unit surface area for an observed relative activity. This curve was generated using two different methods. First two tungsten disks were activated with the same beam parameters used in the cathode activation. The square and circular symbols represent data obtained by repetitively polishing thin layers from the surfaces of the disks and determining the remaining activity relative to the initial activity. The triangles are data from the second method, which involved activating a stack of 25, four μm thick tungsten foils with a beam normal to the surface to produce an activated layer about 110 μm deep, and comparing the activity in each foil to the total activity. A polynomial curve fit to this data is used to convert the raw data described above to mass loss per unit surface area per unit time or discharge.

However, erosion rates are typically expressed as mass loss per coulomb of charge. Since the surface layer activation technique provides spatially resolved measurements of mass loss, the charge transfer through the activated spot must be specified to determine erosion rates in charge transfer units.

In this experiment, the surface layer activation technique was used to measure the cathode erosion rate during operation of the thruster at an argon mass flow rate of 3 g/s with 2 msec long current pulses ranging in amplitude from 8.27 to 14.02 kA, as noted in Table 1. The time-resolved erosion rate in each sequence was monitored using the multichannel analyzer in the multichannel scaling mode described above. The channel dwell time, the total number of shots, and the interval between shots for case are also listed.

Cathode Surface Photomicrography

A 2% thoriated tungsten cathode was polished to a mirror finish with a sequence of abrasives down to a 1 μm diamond paste and then carefully cleaned with Inhibisol and acetone before installation. After evacuating the chamber, the cathode was glow discharged at the conditions listed in Table 2 to remove surface contaminants and oxides, which have been found to strongly affect the characteristic length scales[16,17]. When the tank pressure recovered to 2×10^{-5} torr after 1.5 minutes a single 1 msec discharge was fired at an argon mass flow rate of 3 g/s and a current of 11.2 kA. The voltage trace was much lower than expected for these conditions, and inspection of the thruster subsequently revealed evidence of internal arcing through the mass injection system. Despite these operational problems a substantial amount of the cathode surface was damaged by the arc, providing a fertile ground for a preliminary characterization of cold cathode cratering.

A number of photomicrographs with a magnication of 1000x were taken at each of four axial locations with a scanning electron microscope (SEM). The fossil craters left by the high temperature emission sites were clearly visible and distinct enough from each other and the polished background that the diameter could be measured with a graduated reticle. The diameter was taken to lie inside the crater rim, as illustrated in the 10000x magnification photo in Figure 7.

Experimental Results

Erosion Measurements

In each of the eight tests the activity was found to decrease linearly with time or, equivalently, with the number of shots. The erosion rate listed in column 7 is based on a linear fit to data such as that shown in Figure 5, calibrated in mass loss units with the relationship given by the depth calibration curve. The stated uncertainty is the standard error of the fit and a small additional uncertainty incurred in the calibration, so it reflects primarily statistical scatter in the countrate measurement. Because current density maps are not yet available for these conditions, the erosion rate in charge transfer units listed in column 8 was estimated by assuming that the total measured charge transfer listed in column 2 was uniformly distributed over the 30 cm^2 cathode surface. This erosion rate is plotted as a function of total arc current in Figure 8.

The most striking feature of the data is that it does not scale simply with the charge transfer, but is also a strong funct on of the total current. A very sharp transition to an erosion rate nearly an order of magnitude higher than that at lower currents occurs

between 11.63 and 12.35 kA. The rate then drops to an intermediate value at 14 kA.

A somewhat different picture emerges when the data is plotted on a logarithmic scale, as in Figure 9. Here a very good linear fit is obtained for the data between 10 and 13 kA, with the lower end of the fit intersecting the large error bar bracketing the data point at 8.27 kA. This suggests the following exponential relationship between the erosion rate and discharge current below a critical current lying between 12.35 and 14.01 kA:

$$E_r = (5.63 \times 10^{-9}) \exp(1.84\, J) \qquad (1)$$

Surface Characterization

Figure 10 is a low magnification photograph of the arced cathode surface approximately halfway along the axis which shows a number of damage tracks crossing undisturbed regions. The tracks were found to extend primarily in the axial direction with a slight azimuthal component which caused them to spiral around the cathode, although individual tracks clearly deviate from this general trend. Figure 11 shows the surface at high magnification near the edge of one of these tracks. The craters lie primarily in patches where gross melting has occurred. These tracks were found only in the center of the cathode; at the tip and the base the polished surface had been completely obscured by melting, as exemplified in the photomicrograph of a heavily arced region near the base of the cathode in Figure 12.

Examples of the two classes of arc-produced crater discovered in this study can also be found in Figure 12. The majority of craters were round, as found in vacuum arc photomicrograph studies[18]. However, in each axial position 8-20% of the craters were elliptical with the major axis invariably positioned parallel to the cathode axis.

The dimensions of a total of 1376 craters were measured. The diameters of the round craters and the minor axis lengths of the elliptical craters were found to follow a distribution skewed to the right, as illustrated in Figure 13. The histograms, normal plots, and calculated skewness all indicate that the logarithm of the diameters follows a normal distribution, however. Figures 14, 15, and 16 summarize the variation in the distribution parameters with axial position for the round crater diameters and the minor and major axis lengths of the elliptical craters. The solid lines pass through the mean diameters, the error bars indicate the standard error of the mean, and the broken lines show the standard deviation of the data. The mean diameter of the round craters is about 1 μm, and varies little over the cathode surface. The distribution is very peaked, as indicated by the small standard deviation and a high value for the kurtosis, and the spread also does not vary significantly along the cathode axis. The mean value of the elliptical craters' minor axis length is larger, approximately 1.7 μm, and is relatively constant with position. The distribution is also very narrow, although the spread is greater than that of the round crater diameters and is not as constant with axial position. The distribution of major axis lengths varies little along the length of the cathode, with a mean of about twice that of the minor axis lengths and a spread about 50% higher.

Figure 17 shows the elliptical crater major axis length as a function of the minor axis length for the entire dataset. The two parameters are obviously correlated, with a statistically significant correlation coefficient of 0.36, but it is not clear that a definable relationship exists.

The number of craters per unit area was estimated from each of the photomicrographs and is shown for each axial position in Figure 18. The density is also approximately constant along the cathode, with the highest density occurring at the tip for both classes of craters. The density of elliptical craters is about 20% of the round crater density.

Discussion

The erosion rates measured below 12 kA are the same order of magnitude as previous measurements on cold cathodes[1-9]; however, the transition in behavior occurring at 12 to 13 kA has not been previously reported. Until the current densities are measured for these conditions it is impossible to eliminate a sudden increase in local current density at this current as the cause for this phenomenon. However, it is unlikely that the local charge transfer would increase by an order of magnitude with only a one kA change in total arc current. A more likely explanation is that this point marks the transition to another regime of thruster operation in which additional mass loss mechanisms appear. The current which produces full propellant ionization[19], J_{fi}, for this thruster geometry, propellant, and mass flow rate is calculated to be 12.5 kA, which corresponds to the transition in erosion rate. The full ionization current has been found experimentally to coincide with a number of phenomena such as the appearance of low frequency terminal voltage oscillations or humps in the voltage signal and evolution of the current-voltage characteristic from a linear to a cubic dependence[19]. The current-voltage characteristic measured during this experiment is shown in Figure 19, which shows this change occurring at 11-12 kA. At current levels between 10 and 13 kA many of the measured voltages varied considably from the mean values plotted, and were characterized by non-steady features such as humps after breakdown and sudden drops to lower values during the quasi-steady portion of the current pulse. Recent theoretical and experimental work by Choueiri[20] demonstrates that the growth of a current-driven plasma instability which is responsible for the propellant ionization and heating increases dramatically when the plasma becomes fully ionized, causing a sharp increase in turbulent heating and anomolous resistivity. The correlation of the erosion rate increase with this critical current suggests that mass loss mechanisms other than evaporation and ejection of molten material from the spot regions become active at this point.

However, the consistent observation of cratering and localized melting on cold cathode surfaces indicates that local processes in a number of small emission sites play a major role in cathode mass loss. For this reason, the analytical and experimental effort has centered on the processes involved in crater formation. The widely accepted physical picture of crater formation is that heating by high current density field emission resulting from electric field intensification at a micropoint or dielectric inclusion causes explosive evaporation, which initiates crater formation that continues until some mechanism halts emission or crater growth, at which point a new site erupts to carry the current[21,22]. The current in low-current vacuum arcs is carried by a single luminous spot, and the resulting craters have average diameters which vary linearly with the total arc current, 4.8×10^{-2} μm/A for tungsten[23]. However, there is a critical current at which the arc splits into two or more emission sites, leaving craters with diameters corresponding to the value for the critical current, 250-300 A[18,24], or less, which suggests that some phenomenon limits the total current a single emission site can carry[25,26]. The luminous emission sites move in the retrograde direction opposite the j x B force produced with the self- or external magnetic field in low ambient pressures above a certain critical pressure. This motion is thought to correspond to the extinction of one crater and the ignition of a subsequent emission site on that crater rim or on a micropoint or inclusion further away[21,22].

The following model describes the steady-state crater diameter, assuming that growth ceases when no more energy is available to melt cathode material, which occurs when heat conduction balances joule volume heating and the surface heat inputs. All of the molten cathode material is assumed to be removed from the site by pressure and electro-hydrodynamic forces, leaving a hemispherical crater with an inner surface which advances at the same rate as the melting plane. A spherical geometry is used, with spherically symmetric and purely radial current flow and heat conduction. Thermal conductivity is assumed to be a constant, but electrical resistivity is allowed to vary linearly with temperature. These conditions are described by this one-dimensional, steady-state heat conduction equation and associated boundary conditions:

$$\frac{1}{r^2}\frac{d}{dr}\left(r^2\frac{dT}{dr}\right) + \frac{q_{joule}}{k} = 0$$

$$q_{joule} = j^2\rho_e = \frac{J^2(\rho_{e0} + \alpha T)}{4\pi^2 r^4} \qquad (2)$$

$$T(r_e) = T_m \quad T(\infty) = T_o$$

where r is the radius, T is the temperature, q_{joule} is the joule heating, k is the thermal conductivity, j is the current density, J is the total site current, ρ_e is the electrical resistivity, ρ_{e0} is the constant in resistivity, α is the temperature coefficient of resistivity, r_e is the equilibrium crater radius, T_m is the melting temperature, and T_o is the undisturbed temperature far from the site. The solution to this equation after application of the

boundary conditions yields the radial temperature distribution in the cathode surrounding the hemispherical crater. To determine r_e from this relation, the additional condition of heat transfer at the surface must be supplied. To obtain a first estimate the simple case of an insulating surface was examined. For this condition the equilibrium crater radius is given by

$$r_e = \frac{J\left[\frac{\alpha}{4\pi^2 k}\right]^{1/2}}{\cos^{-1}\left[\frac{(T_o - \rho_{eo}/\alpha)}{(T_m - \rho_{eo}/\alpha)}\right]} \qquad (3)$$

which shows the linear relationship between radius and site current that is observed experimentally in vacuum arcs. For tungsten this relationship is $r_e = (0.183)\,J$, with J in A and r_e in μm, which is about four times higher than that given by Daalder on the basis of one measurement[23]. This length scale may be underestimated because surface heating was neglected, but this is offset to a certain extent by the assumptions that all of the molten material is removed and that site operation actually lasts long enough for the crater to reach thermal equilibrium.

The heavy arcing and gross melting at the base and tip of the cathode and distinct arc tracks in the center suggest that the degree of coverage depends on the current density, since cathode current densities tend to peak at the base and tip. It is probable that the motion of the arc spots results in molten tracks containing the discrete emission sites everywhere, and that variations in appearance along the cathode simply reflect differing numbers of active spots. However, one would also expect the crater density to follow the axial current density variations. The fact that the data in Figure 18 do not support this conclusion may be attributable to an underestimate of the crater density in the heavily arced regions at the tip and base, where multiple track crossings may have covered previous cratering or surface tension in grossly melted areas may have resulted in the smoothing of fossil crater remains.

The observation of log-normal distributions of round crater diameters and elliptical crater minor axis lengths agrees with previous experiments conducted on other metals in vacuum arcs[18]. The skewed distributions are not unexpected, since the distribution is naturally truncated on the left by the physical requirement that the lengths be positive and possibly because very small craters were undetectable or were more susceptible to smearing by surface tension forces in molten areas.

Several possible explanations for the formation of elliptical craters exist. For instance, such emission sites might erupt around elongated dielectric inclusions. However, the alignment of the craters' major axes with the Lorentz force strongly suggests that the elliptical craters are a result of spot motion parallel or anti-parallel to the magnetic field. If the minor axis length is identified as the characteristic dimension of the emitting site which is a linear function of the site current, comparison of the means indicates that the elliptical craters carry more current on average than the round craters. The relationship given by equation (3) yields 4.7 A compared to 3.0 A. The sites with higher currents apparently have a higher probability of moving continuously rather than jumping to a new discrete emission site. The correlation between the minor axis length (or current carried by the site) and the major axis length (or extent of travel) suggests that craters carrying higher currents will travel a longer distance on average before extinction. Both observations lead to the conclusion that the current per site affects either the velocity of motion or the site lifetime. However, the minor axis length may not correspond to the emission site diameter, but instead may simply reflect the fact that a moving heat source will heat the center of the path more than the endpoints. If this is the case, it is impossible to identify a characteristic length scale for the elliptical craters.

The measured round crater diameters provide a relatively unambiguous length scale for cold cathode cratering, although a small uncertainty is introduced in the definition of crater diameter. As previous experimentation on other metals and the theoretical model show, the crater diameter can be associated with a current for that site, so the mean crater diameter corresponds to the most probably site current. The spread in the distribution may be identified with a statistical variation in the current carried per emission site. The most remarkable implication of the data presented here is how little the current per site deviates from the average over the cathode surface. The discharge apparently draws current from the surface in exactly the same fashion, regardless of how discharge parameters such as current density, and plasma density, temperature, and velocity vary along the axis.

Another important observation is that the diffuse MPD discharge extracts current from sites carrying much less than the 250-300 A limiting current. An estimate of the site lifetime can be obtained by assuming a uniform macroscopic current density of 373 A/cm^2 for the 1 msec arc and a crater density on the order of that measured, 10^6/cm^2. This yields a charge transfer per crater of 3.8×10^{-7} C. If each crater carried on average 3.0 A, the crater lifetime would then be about 130 nsec. This is in the range of site lifetimes measured by Puchkaryov on tungsten point cathodes[27].

Conclusions

Surface layer activation has now been demonstrated as a mature technology capable of rapidly producing high accuracy, spatially and temporally resolved mass loss data that can be used to characterize MPD thruster cathode erosion. The photomicrographic study, although not conducted under conditions of ideal thruster operation, illustrates that the technique can be used to obtain fundamental data on the length scales characteristic of cold cathode erosion damage. The data presented above permit several tentative conclusions concerning cold cathode operation.

The measured erosion rates offer the message that cathode erosion is one of many MPD thruster characteristics that undergoes a change when the full ionization current is reached, although it is unclear at this point whether it is proper to characterize this transition as a change from an exponential dependence of erosion rate on current or a sudden dramatic increase in cathode erosion. Subsequent erosion tests at different mass flow rates will be conducted to verify that the transition is correlated with J_{fi} and to test the exponential relationship at currents below J_{fi}, and magnetic field probing will be used to determine if the increased mass loss is due to an unexpected increase in local current density or to the unleashing of additional erosion mechanisms.

The large database of measurements obtained from the preliminary test of cathode surface photomicrography indicates that the characteristic dimension of a discrete emission site is on the order of 1 μm, and is surprisingly uniform over the cathode surface. The simple thermal model of crater formation yields a linear relationship between site current and the crater diameter, and comparison of this result with the measured diameters and crater densities suggests that typical emission sites on the cold cathode of an MPD thruster carry only a few amps each for time periods on the order of 100 nsec. The existence of elliptical craters is interpreted as a manifestation of spot motion. Subsequent applications of this method will be aimed at confirming the results suggested by this test and studying differences above and below the full ionization current.

Acknowledgements

The authors would like to acknowledge the assistance and advice of Elaine Lenk in the Biology Depa tment's Scanning Electron Microscope Laboratory, the staff o the Princeton University Cyclotron Facility, and Ruth Caswell '88, who provided invaluable aid in obtaining the crater length scale data.

References

1. Polk, J.E., von Jaskowski, W., Kelly, A.J., and Jahn, R.G., "Measurement of MPD Thruster Erosion Using Surface Layer Activation," AIAA Journal of Power and Propulsion, Vol. 3, No. 1, pp 33-38, 1987.
2. Polk, J.E., Kelly, A.J., and Jahn, R.G., "MPD Thruster Erosion Research," AIAA Paper 87-0999, May 1987.
3. Schrade, H.O., Auweter-Kurtz, M., and Kurtz, H.L., "Cathode Erosion Studies on MPD Thrusters," AIAA Paper 85-2019, Oct. 1985.
4. Uematsu, K., "Effect of Electrode Configuration on MPD Arcjet Performance," AIAA Paper 84-11, July 1984.
5. Kagaya, Y., Yokoi, Y, Tahara, H., and Yoshikawa, T., "Thrust Performance and Current Distribution in a Quasi-steady MPD Arcjet," AIAA Paper 84-31, July 1984.
6. Yoshikawa, T., Kagaya, Y., Yokoi, Y., and Tahara, H., "Performance Characteristics of Quasi-steady MPD

Thrusters," AIAA Paper 84-58, July 1984.
7. Kuriki, K., Uematsu, K., and Morimoto, S., "MPD Arcjet Performance with Various Propellants," AIAA Paper 82-1885, Nov. 1982.
8. Tahara, H., Kagaya, Y., and Yoshikawa, T., "Quasi-steady MPD Arcjets with Applied Magnetic Fields," AIAA Paper 85-2001, Sept. 1985.
9. Yoshikawa, T., and Kagaya, Y., "Thrust and Efficiency of New K-III MPD Thruster," AIAA Paper 82-1887, Nov. 1982.
10. Kaplan, D.I., and Jahn, R.G., "Performance Characteristics of Geometrically Scaled Magnetoplasmadynamic (MPD) Thrusters," Mechanical and Aerospace Engineering Dept., Princeton University, Princeton, NJ Report 1632-T, 1983.
11. Polk, J.E., Kelly, A.J., and Jahn, R.G., "Advanced Electric Propulsion MPD," Technical Progress Report 85, AF Contract F 04 611-85-c-0021. Nov. 1986.
12. Conlon, T.W., "Doping Surfaces with Radioactive Atoms--for Research and Industry," Contemp. Phys., Vol. 23, No. 4, pp 353-369, 1982.
13. Quittner, P., Gamma Ray Spectroscopy, Halsted Press, 1972.
14. Schonfeld, E., et. al., "Determination of Nuclide Concentrations in Solutions Containing Low Levels of Radioactivity by Least-Squares Resolution of the Gamma-Ray Spectra," Nuclear Instruments and Methods, Vol. 45, pp 1-21, 1966.
15. Schonfeld, E., "ALPHA-M, An Improved Computer Program for Determining Radioisotope Concentrations by Least Squares Resolution of the Gamma-Ray Spectra," ORNL-3975, Sept. 1966.
16. Guile, A.E., and Juttner, B., "Basic Erosion Processes of Oxidized and Clean Metal Cathodes by Electric Arcs," IEEE Trans. on Plasma Science, Vol. PS-8, No. 3, pp. 259-269 Sept. 1980.
17. Guile, A.E., and Hitchcock, A.H., "Oxide Films on Arc Cathodes and Their Emission and Erosion," J Phys. D: Appl. Phys., Vol. 8, pp 663-668, 1975.
18. Daalder, J.E., "Diameter and Current Density of Single and Multiple Cathode Discharges in Vacuum," IEEE Trans. Pow. App. Syst. PAS-93, pp 1747-1758, 1974.
19. Choueiri, E.Y., Kelly, A.J., and Jahn, R.G., "The Manifestation of Alfven's Hypothesis of Critical Ionization Velocity in the Performance of MPD Thrusters," AIAA Paper 85-2037, Oct. 1985.
20. Choueiri, E.Y., Kelly, A.J., and Jahn, R.G., "Current-Driven Instabilities in an Electromagnetically Accelerated Plasma," AIAA Paper 88-042, Oct. 1988.
21. Hantzsche, E., "Cathode Processes in Vacuum Arcs," Proc. Int'l Conf. on Phenomena in Ionized Gases, vol. 2, p. 121, 1977.
22. Ecker, Gunter, "The Vacuum Arc--A Phenomenon of Many Aspects," IEEE Trans. Plasma Sci., Vol. PS-4, No. 4, pp. 218-227, Dec. 1976.
23. Daalder, J.E., "Cathode Erosion of Metal Vapour Arcs in Vacuum," PhD. Thesis, Eindhoven Technical University, Eindhoven, The Netherlands, 1978.
24. Kimblin, C.W., "Erosion and Ionization in the Cathode Spot Regions of Vacuum Arcs," J. Appl. Phys., Vol. 44, No. 7, pp. 3074,3081, July 1973.
25. Hantzsche, E., Beitr. Plasmaphys., Vol. 12, p. 245, 1972.
26. Daalder, J.E., Eindhoven Technical University, Report No. ISBN 90 6144 033 5, Eindhoven, The Netherlands, 1973.
27. Puchkaryov, V.F., and Proskurovsky, D.I., "A Study of the Cathode-Spot Operation of Tungsten Point Cathodes in the Range of Threshold Arc Currents," IEEE Trans. Plasma Sci., Vol. PS-13, No. 5, pp. 257-260, Oct. 1985.

Table 1: Conditions and Results of Erosion Experiments

	m = 3 g/s	Propellant: Argon		Pulse Duration = 2 msec		
J (kA)	Charge Transfer (C/shot)	Number of Discharges	Interval b/t Shots (s)	Dwell Time (s)	Erosion Rate ($\mu g/cm^2$-shot)	Erosion Rate ($\mu g/C$)
8.27 ± .002	18.59 ± .03	250	30	30	-.2 ± .5	-.3 ± .9
10.30 ± .02	22.20 ± .02	250	30	30	.9 ± .4	1.1 ± .5
10.36 ± .01	22.36 ± .01	1000	30	100	.98 ± .08	1.3 ± .1
11.10 ± .03	22.81 ± .01	250	30	30	2.4 ± .6	3.1 ± .8
11.63 ± .01	23.131 ± .006	250	30	30	6.4 ± .6	8.3 ± .8
12.35 ± .009	23.578 ± .009	250	30	30	45 ± 1	58 ± 2
14.01 ± .02	25.36 ± .05	93	30	75	26 ± 2	30 ± 2
14.02 ± .07	25.37 ± 04	48	30	30	39 ± 7	50 ± 9

Table 2: Glow Discharge Conditions

Argon Flow Rate (g/s)	0.08
Tank Pressure (mTorr)	40
Voltage (V)	1000
Current (mA)	25-500
Duration (sec)	240

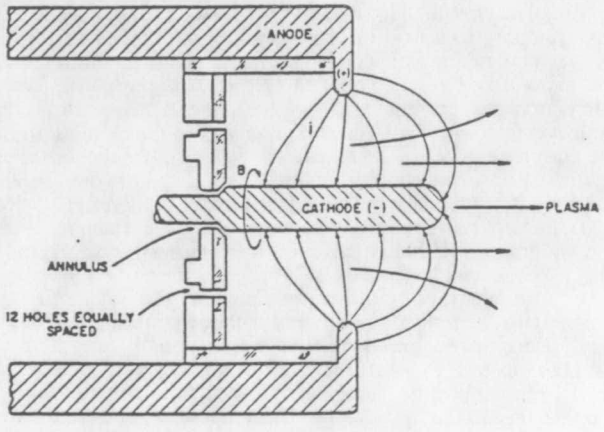

Fig. 1: Half-scale benchmark thruster.

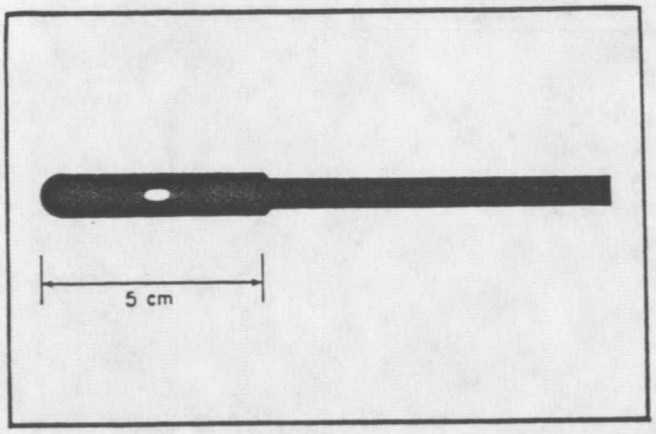

Fig. 2: Autoradiograph of the activated cathode.

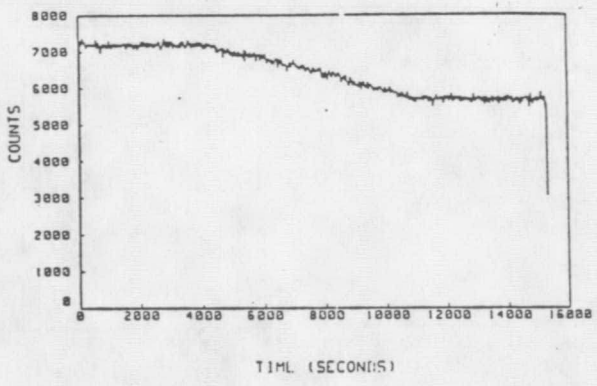

Fig. 5: Activity time history produced by multi-channel scaling.

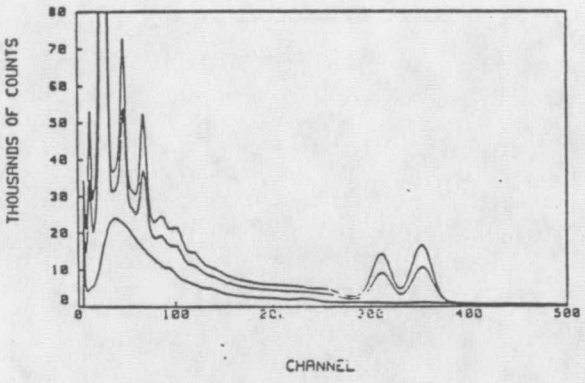

Fig. 3: Typical gamma ray spectra.

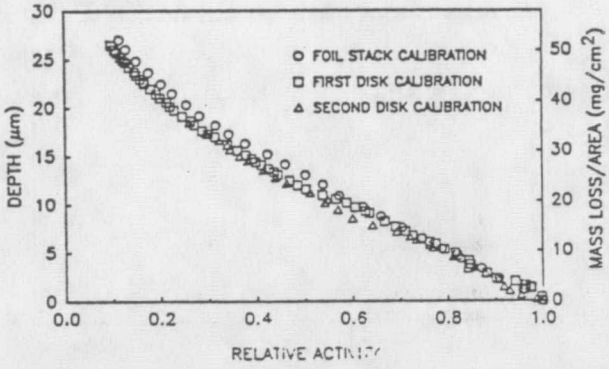

Fig. 6: Depth calibration curve for ^{184}Re.

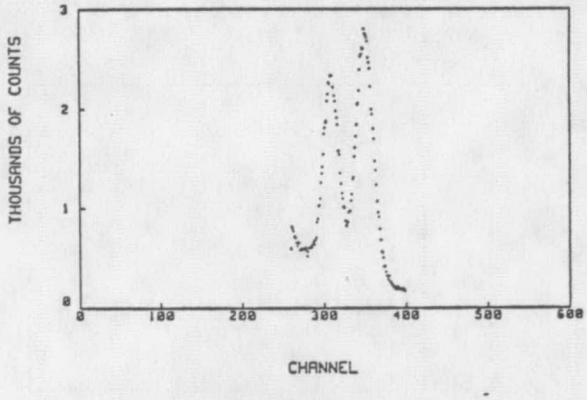

Fig. 4: Spectral region isolated with upper- and lower-level pulse-height discriminators.

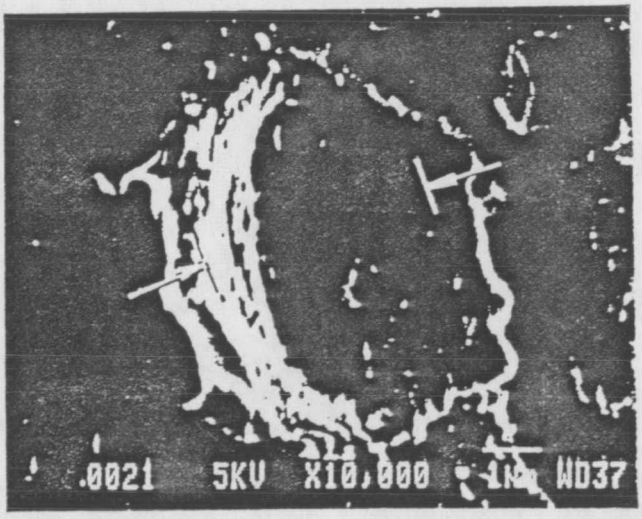

Fig. 7: Photomicrograph of crater with diameter marked.

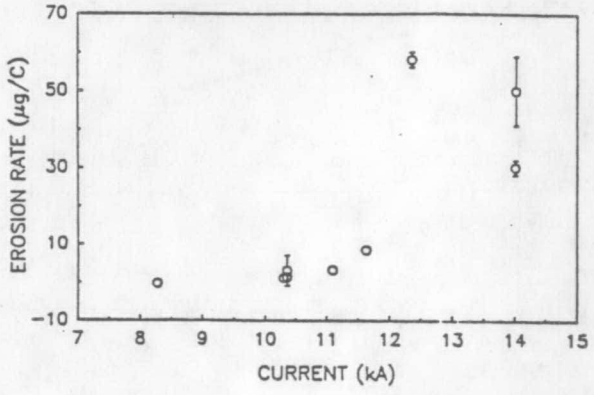

Fig. 8: Variation of cathode erosion rate with total thruster current.

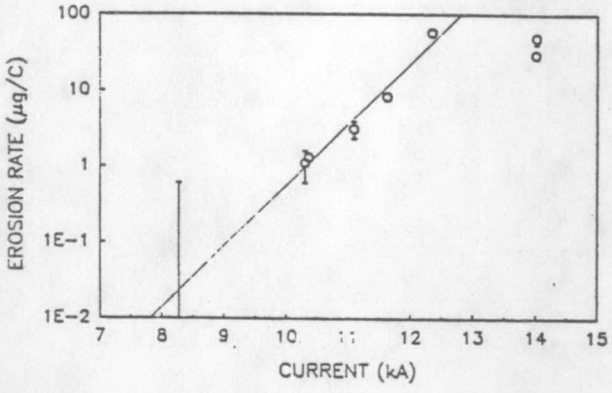

Fig. 9: Logarithmic plot of cathode erosion rate as a function of total thruster current.

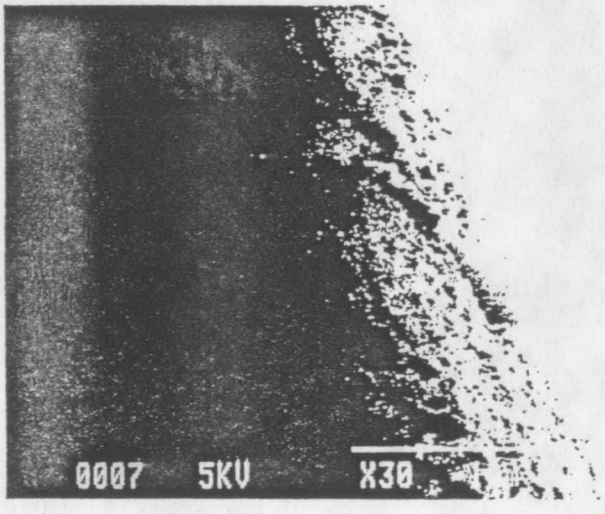

Fig. 10: Photomicrograph of arc tracks.

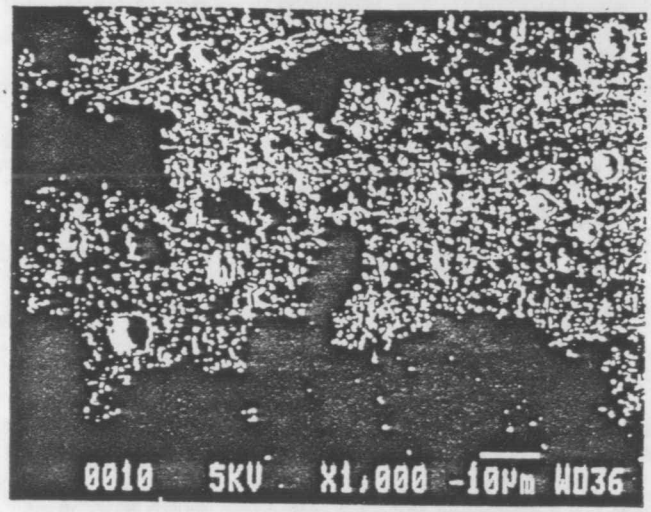

Fig. 11: Photomicrograph of arc track edge.

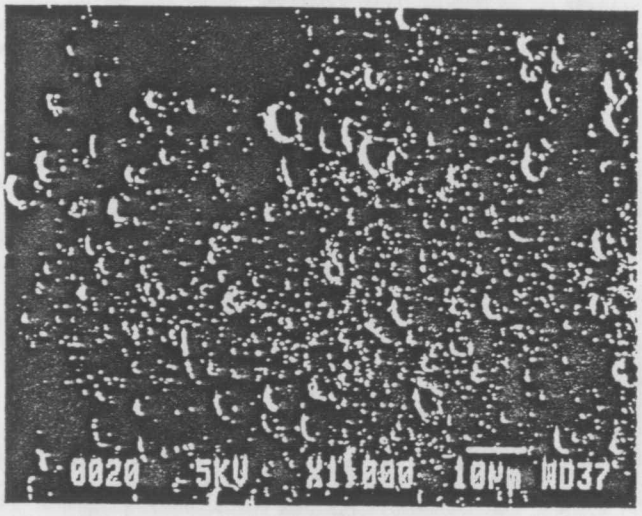

Fig. 12: Photomicrograph of heavily arced region.

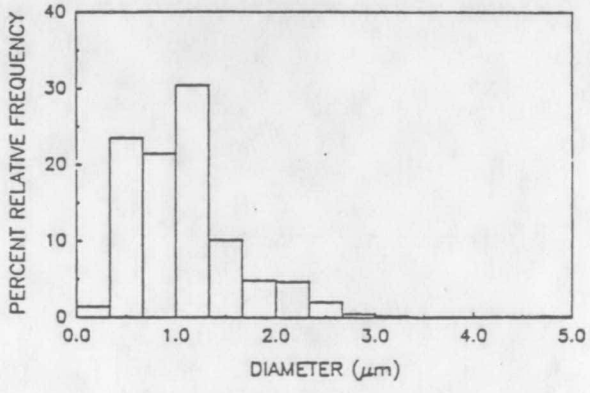

Fig. 13: Distribution of round crater diameters.

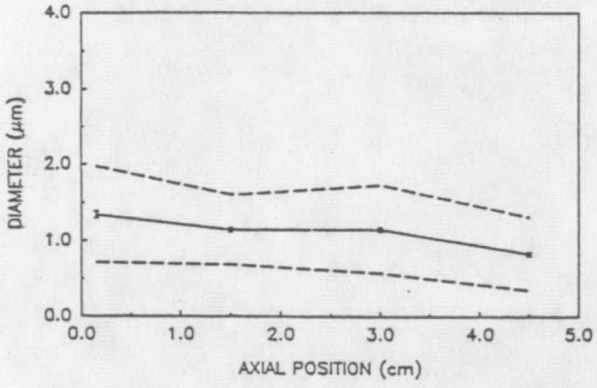

Fig. 14: Variation of round crater diameter mean and standard deviation with axial position.

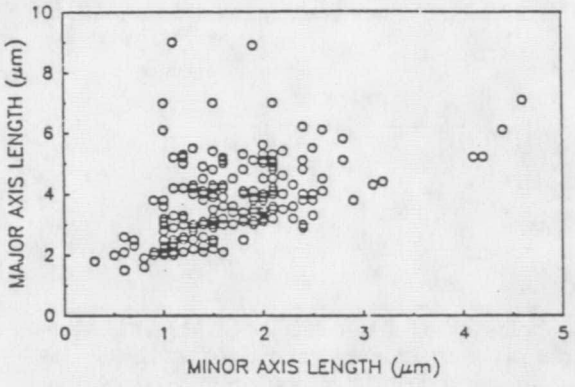

Fig. 17: Elliptical crater major axis length as a function of minor axis length.

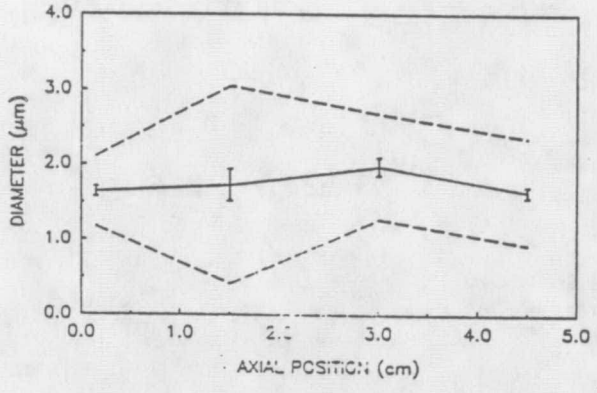

Fig. 15: Variation of elliptical crater minor axis length mean and standard deviation with axial position.

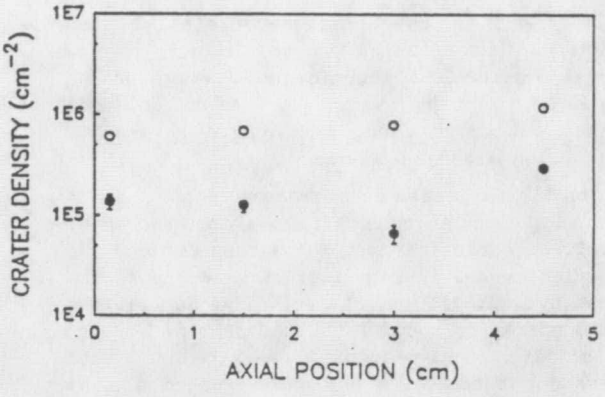

Fig. 18: Variation of crater density with axial position.

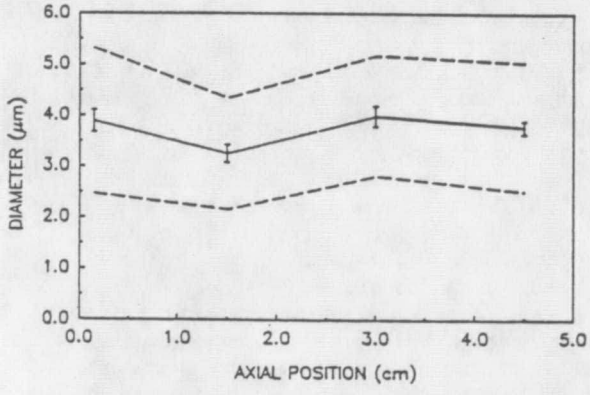

Fig. 16: Variation of elliptical crater major axis length mean and standard deviation with axial position.

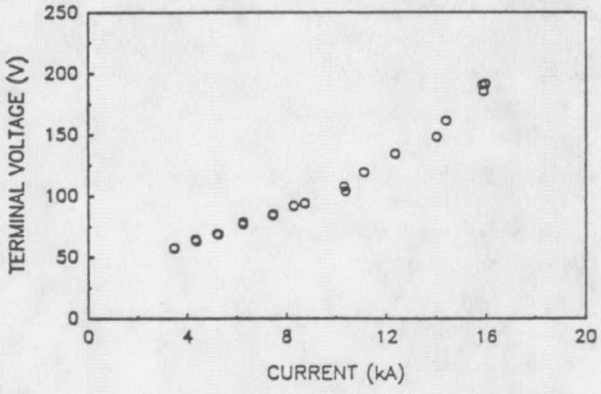

Fig. 19: Voltage-current characteristic for argon, 3 g/s.